

On Modeling Viscous Damping in Nonlinear Dynamic Analysis of Base-Isolated Reinforced Concrete Buildings



D.R. Pant & A.C. Wijeyewickrema

Tokyo Institute of Technology, Japan

SUMMARY:

The effects of modeling viscous damping on the response indicators of base-isolated reinforced concrete buildings subjected to earthquake ground motions are investigated using a three-story building previously tested on a shaking table. Three-dimensional finite element simulations are carried out, using many different approaches of applying viscous damping to the superstructure of the building. The approaches considered here are developed within the framework of Rayleigh damping. Nonlinear behavior of the superstructure as well as the isolation system is considered in the analyses. It is recommended to use Rayleigh damping where the damping ratio is carefully selected and the coefficients multiplying the mass and stiffness matrices are calculated from the frequencies of the building based on the post-elastic stiffness of the isolation system. Alternatively, stiffness-proportional damping where the coefficient multiplying the stiffness matrix is calculated from the frequency of the superstructure for a fixed-base condition can be used.

Keywords: Base isolation, nonlinear analysis, Rayleigh damping, shaking table test

1. INTRODUCTION

Modeling viscous damping is a challenging task for base-isolated buildings which consist of two subsystems viz. the isolation system and the superstructure, with substantially different energy dissipation properties. It is logical to prescribe viscous damping separately for the isolation system and the superstructure, where the use of viscous damping in the isolation system can be avoided by using hysteretic models of bearings to account for all the energy dissipation. On the other hand, the application of viscous damping to the superstructure alone can be done using various approaches within the Rayleigh damping framework, where damping matrix \mathbf{c} is given as,

$$\mathbf{c} = a_0 \mathbf{m} + a_1 \mathbf{k}, \quad (1.1)$$

where \mathbf{m} is the mass matrix, \mathbf{k} is the stiffness matrix, and a_0 and a_1 are the damping coefficients. The damping ratio for the n^{th} mode of a structure ξ_n is defined as,

$$\xi_n = \frac{a_0}{2\omega_n} + \frac{a_1 \omega_n}{2}, \quad (1.2)$$

where ω_n is the frequency of the n^{th} mode. The coefficients a_0 and a_1 are determined assuming the same damping ratio ξ for two selected modes as,

$$a_0 = \xi \frac{2\omega_i \omega_j}{\omega_i + \omega_j}, \quad a_1 = \xi \frac{2}{\omega_i + \omega_j}, \quad (1.3)$$

where ω_i and ω_j are the frequencies of mode i and mode j , respectively. The two modes i and j are chosen to ensure nearly the same amount of damping for all the modes significantly contributing to the response of the structure (Chopra 2007). Typically, ω_i is selected to be the frequency of the first mode and ω_j corresponds to a higher mode. Mass-proportional damping where $\mathbf{c} = a_0 \mathbf{m}$ and $a_0 = 2\xi\omega_i$; and stiffness-proportional damping where $\mathbf{c} = a_1 \mathbf{k}$ and $a_1 = 2\xi/\omega_i$, can be viewed as special cases of Rayleigh damping.

Conventionally, the damping matrix \mathbf{c} is computed using Rayleigh damping based on *initial elastic properties* of the system. This practice is based on the notion that energy dissipation due to viscous damping is negligible, compared with the much higher energy dissipation due to material nonlinearity in the inelastic range. However, conventional application of Rayleigh damping could lead to unrealistically large damping forces, resulting in an unconservative design (Hall 2006). While the issue of modelling viscous damping has been explored extensively for fixed-base buildings (see for example Léger and Dussault 1992, Charney 2008, and Erduran 2012), it is only recently that the base-isolated buildings have been considered (see Hall 2006 and Ryan and Polanco 2008). Hall (2006) studied the effects of mass-proportional damping and stiffness-proportional damping using a rigid superstructure model. Ryan and Polanco (2008) recommended the application of stiffness-proportional damping instead of Rayleigh damping to the superstructure of the building but their study was based on two-dimensional models of the buildings assuming linear elastic behavior of the superstructure. Stiffness-proportional damping was also used by Pant and Wijeyewickrema (2012) to evaluate the performance of a base-isolated reinforced concrete (RC) building subjected to seismic pounding using three-dimensional nonlinear finite element (FE) models. However, the effects of modeling viscous damping on the structural response of the building were not discussed in that study. Therefore, a systematic study investigating the effects of modeling viscous damping on the important response indicators of base-isolated buildings such as floor displacements, floor accelerations and story shear forces, using rigorous three-dimensional FE models, is needed. In addition, none of these previous studies have compared numerical analysis results with the results from experiments or instrumented buildings.

In the present study, the consequences of modeling viscous damping in time-history analysis of base-isolated RC buildings by using various approaches based on the Rayleigh damping framework, are investigated. Existing shaking table test results of a three-story base-isolated building, where the superstructure was shaken strongly but did not undergo significant inelastic excursions, are compared with the numerical analysis results to arrive at the appropriate technique for modeling viscous damping. In these numerical simulations, energy dissipation due to inelastic material behavior of the superstructure was simulated using well-established material models, while the viscous damping was applied to the superstructure using many different approaches. All the energy dissipation in the isolation system was explicitly modeled using bilinear hysteretic models of bearings.

2. BENCHMARK BUILDING AND NUMERICAL MODELING

The base-isolated benchmark building used to compare numerical analysis results is a 0.4 scale model of a three-story two-bay by one-bay RC structure built in Japan (Fig. 2.1). To maintain proper scaling, packets of lead billets were tied down to each slab and the total weight of the model was 400 kN. Three phases of shaking table tests were carried out following initial system identification tests including the static pull-back tests. However, due to improper calibration of loadcells during the first static pull-back test, localized cracking was observed especially in first-floor beam-column joints (Clark et al. 1997). In the first phase of the shaking table tests, the structure was braced in the transverse direction as well as the longitudinal direction to enable comparison of various isolation systems by avoiding damage to the superstructure. Design-level 1 and design-level 2 earthquake excitations, according to Japanese practice were used as input in this stage. In the second phase of the

tests, the model was braced only in the transverse direction and the two design-level earthquakes were run again, followed by very high-intensity motions intended to cause damage to the structure. In the final phase, the model was repaired and moderate-intensity motions were applied. It is noted that in all the tests, the earthquake excitation was only in the longitudinal direction. This study focuses on the second phase of the tests where design-level earthquakes were used. In this phase, identical 176 mm diameter high damping rubber bearings with twenty 2.2 mm thick rubber layers alternating with 1 mm thick steel shims were used under each of the six column bases.

Design-level 2 tests which led to yielding in the RC frame during the tests are considered in the present study. In these tests, recordings of the 1940 El Centro, 1968 Tokachi-oki, and 1979 Miyagiken-oki earthquakes were run at an intensity corresponding to the full-scale peak velocity of 50 cm/sec (corresponding to the design-level 2 earthquake) and are referred to as ELC-50, HACH-50, and MIYA-50, respectively. One additional excitation that represented the design forces typically specified by the US codes was also used in these tests. The excitation referred to as ELC-S1, is a synthetic record generated from the 1940 El Centro earthquake recording. The sequence of excitation was in the following order: ELC-S1, ELC-50, HACH-50, and MIYA-50.

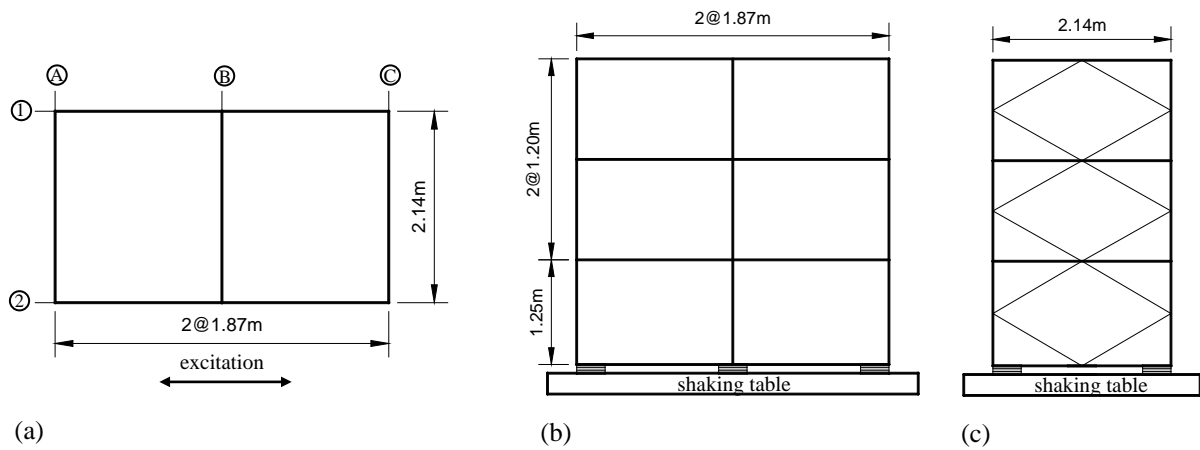


Fig. 2.1. Geometry of the three-story building tested on shaking table: (a) plan; (b) elevation along longitudinal direction; and (c) elevation along transverse direction (note that no braces were used along grid line B).

2.1. Modeling of structural elements

Three-dimensional FE model of the building was developed in OpenSees (2010). Beams and columns were modeled using force-based, Euler-Bernoulli fiber beam-column elements that account for the spread of inelasticity along the length of the element. For concrete the modified Kent and Park model (Park et al. 1982) was used in compression and an initial linear elastic branch together with a linear softening branch up to zero stress was used in tension. The model proposed by Yassin (1994) was used to account for concrete damage and hysteresis. For reinforcing steel, the constitutive model of Menegotto and Pinto (1973), which includes strain hardening and the Bauschinger effect, was used. In this study, the strain-hardening ratio is taken as 1%. Bearings were modeled using elastomeric bearing elements with a bilinear hysteretic model used to represent the lateral force-deformation relationship of each element and to simulate all the energy dissipation in the isolation system. The parameters of the bilinear hysteretic model for each element as determined from the component test results of a bearing that was similar to the ones used in the building, are initial stiffness $K_1 = 1,167.5$ kN/m, post-elastic stiffness $K_2 = 300$ kN/m, and yield force $F_y = 3.94$ kN. The vertical force-deformation relationship of each element was simulated using a linear elastic compression-only spring with a stiffness $K_v = 338,000$ kN/m. The standard horizontal characteristic test of the bearing at 100% shear strain level and an axial load of 78.5 kN was reproduced quite well using these properties as shown in Fig. 2.2.

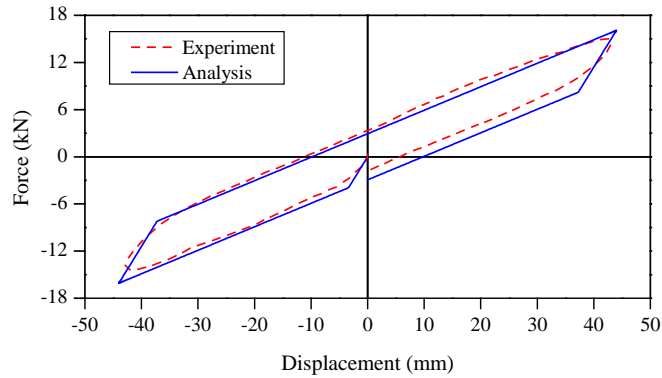


Fig. 2.2. Hysteretic loop of the bearing for one cycle of displacement at 100% shear strain level. Experimental curve is reproduced after Clark et al. (1997).

2.2. Modeling of viscous damping

Viscous damping was applied only to the superstructure of the building using many different approaches of computing the damping matrix \mathbf{c} that cover a wide range of options available in many existing FE programs (Table 2.1). The relevant frequencies as obtained from modal analyses are also shown in Table 2.1. Since the modal damping values could not be estimated reasonably well during the test (Clark et al. 1997), numerical simulations were performed using damping ratio $\xi = 1\%$, 2% , 3% , 4% , and 5% . This also enables the investigation of the effects of damping ratio on the analysis results. The approaches considered here depend on:

- (1) *Damping*: Rayleigh, mass-proportional or stiffness-proportional damping.
- (2) *Damping coefficients* a_0 , a_1 : The damping coefficients a_0 and a_1 are constant throughout the analysis (based on the initial stiffness) or updated in each analysis step (based on the tangent stiffness).
- (3) *Basis for computing* a_0 , a_1 : Modes of deformation chosen and the structural model considered for modal analysis to calculate frequencies necessary for the evaluation of damping coefficients.
- (4) *Stiffness matrix*: Initial or tangent stiffness matrix used in Eq. (1.1).

The approaches are grouped as follows:

- (1) Group A: Rayleigh damping; damping coefficients are constant and calculated from modal analysis of the superstructure for a fixed-base condition (Approaches 1–4).
- (2) Group B: Rayleigh damping; damping coefficients are constant and calculated from modal analysis of the base-isolated building with initial stiffness of the isolation system (Approaches 5–8).
- (3) Group C: Rayleigh damping; damping coefficients are constant and calculated from modal analysis of the base-isolated building with post-elastic stiffness of the isolation system (Approaches 9–12).
- (4) Group D: Rayleigh damping; damping coefficients are updated and calculated from modal analysis of the base-isolated building (Approaches 13–16).
- (5) Group E: Mass-proportional damping (Approaches 17–20).
- (6) Group F: Stiffness-proportional damping; damping coefficient is constant and calculated from modal analysis of the superstructure for a fixed-base condition (Approaches 21–22).
- (7) Group G: Stiffness-proportional damping; damping coefficient is calculated from modal analysis of the base-isolated building (Approaches 23–28).

Table 2.1. Different approaches of modeling viscous damping.

Approach	Group	Damping	Damping coefficients a_0, a_1	Basis for computing a_0, a_1		Stiffness matrix	ω_i (rad/s)	ω_j (rad/s)
				Modes i, j	Structural model			
1	A	Rayleigh	Constant	1, 3	SS	Initial	37.14	66.62
2	A	Rayleigh	Constant	1, 3	SS	Tangent	37.14	66.62
3	A	Rayleigh	Constant	1, 4	SS	Initial	37.14	130.62
4	A	Rayleigh	Constant	1, 4	SS	Tangent	37.14	130.62
5	B	Rayleigh	Constant	1, 3	BIB-I	Initial	12.61	60.18
6	B	Rayleigh	Constant	1, 3	BIB-I	Tangent	12.61	60.18
7	B	Rayleigh	Constant	1, 4	BIB-I	Initial	12.61	64.03
8	B	Rayleigh	Constant	1, 4	BIB-I	Tangent	12.61	64.03
9	C	Rayleigh	Constant	1, 3	BIB-P	Initial	6.58	58.58
10	C	Rayleigh	Constant	1, 3	BIB-P	Tangent	6.58	58.58
11	C	Rayleigh	Constant	1, 4	BIB-P	Initial	6.58	64.03
12	C	Rayleigh	Constant	1, 4	BIB-P	Tangent	6.58	64.03
13	D	Rayleigh	Updated	1, 3	BIB	Initial	—	—
14	D	Rayleigh	Updated	1, 3	BIB	Tangent	—	—
15	D	Rayleigh	Updated	1, 4	BIB	Initial	—	—
16	D	Rayleigh	Updated	1, 4	BIB	Tangent	—	—
17	E	Mass prop.	Constant	1	SS	—	37.14	—
18	E	Mass prop.	Constant	1	BIB-I	—	12.61	—
19	E	Mass prop.	Constant	1	BIB-P	—	6.58	—
20	E	Mass prop.	Updated	1	BIB	—	—	—
21	F	Stiffness prop.	Constant	1	SS	Initial	37.14	—
22	F	Stiffness prop.	Constant	1	SS	Tangent	37.14	—
23	G	Stiffness prop.	Constant	1	BIB-I	Initial	12.61	—
24	G	Stiffness prop.	Constant	1	BIB-I	Tangent	12.61	—
25	G	Stiffness prop.	Constant	1	BIB-P	Initial	6.58	—
26	G	Stiffness prop.	Constant	1	BIB-P	Tangent	6.58	—
27	G	Stiffness prop.	Updated	1	BIB	Initial	—	—
28	G	Stiffness prop.	Updated	1	BIB	Tangent	—	—

3. COMPARISON OF TEST AND NUMERICAL ANALYSIS RESULTS

Nonlinear time-history analysis of the building was carried out using OpenSees (2010) for a single continuous sequence of concatenated records ELC-S1, ELC-50, HACH-50, and MIYA-50 using the 28 approaches of modeling viscous damping. The $P-\Delta$ effect for the superstructure as well as the isolation system was included in the analysis to consider geometric nonlinearity effects. Numerical analysis results only for the weakest (i.e., ELC-S1) and the strongest (i.e., MIYA-50) excitations (Fig. 3.1) are discussed in this paper, for brevity. The selected response indicators are relative floor displacements, absolute floor accelerations, and story shear forces. To enable the comparison of various approaches of modeling damping, the error E_n of the peak value of the response indicator representing displacement, acceleration or shear force at n^{th} story was calculated as,

$$E_n = \left| \frac{N_n - T_n}{T_n} \right|, \quad n = 0 \text{ (base), } 1, 2, 3 \text{ (roof)}, \quad (3.1)$$

where N_n and T_n are the peak values of numerical analysis and test results, respectively of the response indicator at n^{th} story. Maximum of E_n values at all the stories for various damping ratios and approaches of modeling viscous damping are shown in Fig. 3.2 and Fig. 3.3 for the ELC-S1 excitation and the MIYA-50 excitation, respectively. Maximum errors when the viscous damping was not considered in the analysis are also shown for comparison purposes. Figures 3.2 and 3.3 show that the error trends using various approaches are nearly the same for the ELC-S1 and MIYA-50 excitations with a few exceptions, especially in Group E (mass-proportional damping). In general, the errors under the stronger excitation are smaller than those under the weaker excitation. It is noted that the peak inter-story drift ratios were found to be relatively small at 0.12% and 0.2% for the ELC-S1 and MIYA-50 excitations, respectively. Although there are differences between errors under the two excitations, the superstructure does not experience enough damage to significantly affect the dynamic characteristics of the building under both the excitations. Therefore, unless specified otherwise, the discussion from here onwards will be focused on the response under the MIYA-50 excitation.

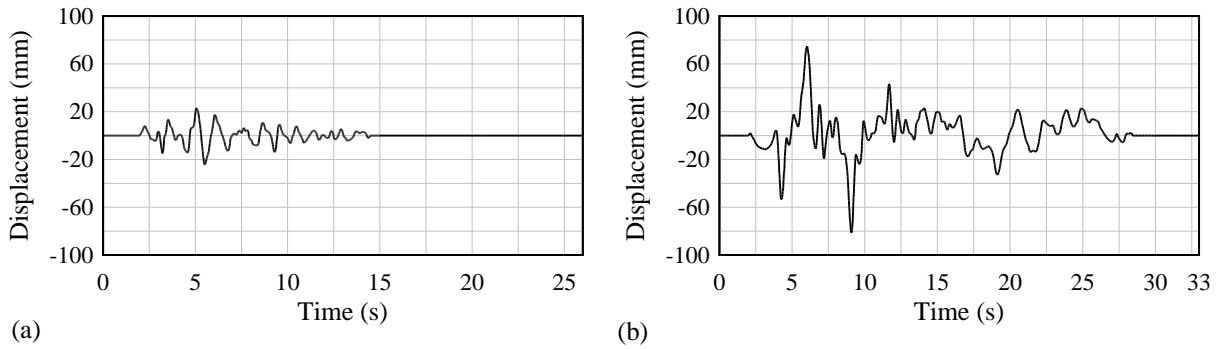
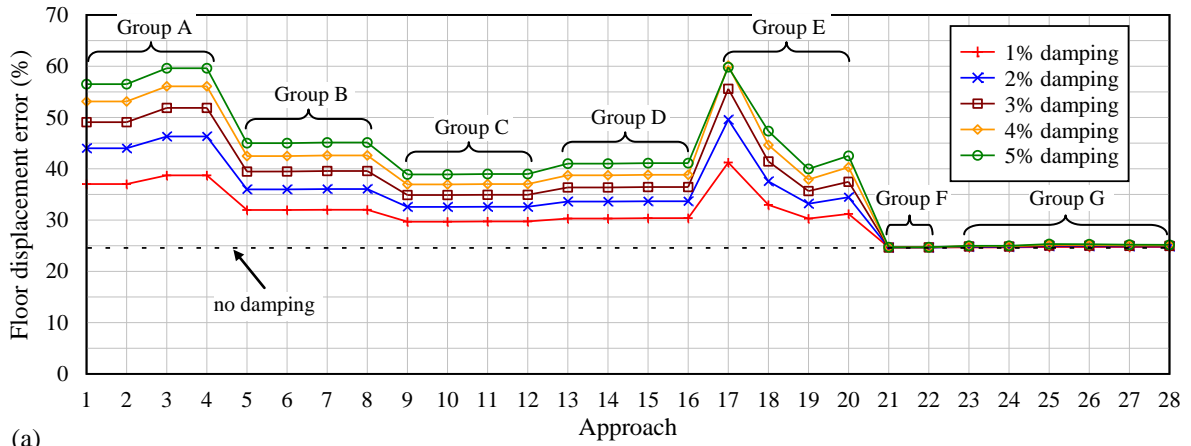
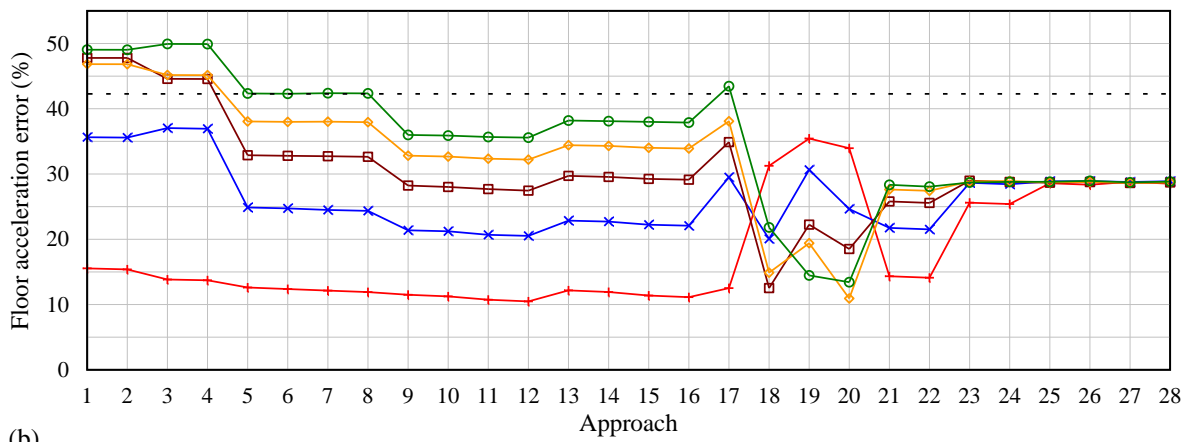


Fig. 3.1. Displacement time histories of the input motions: (a) ELC-S1 and (b) MIYA-50 Clark et al. (1997).

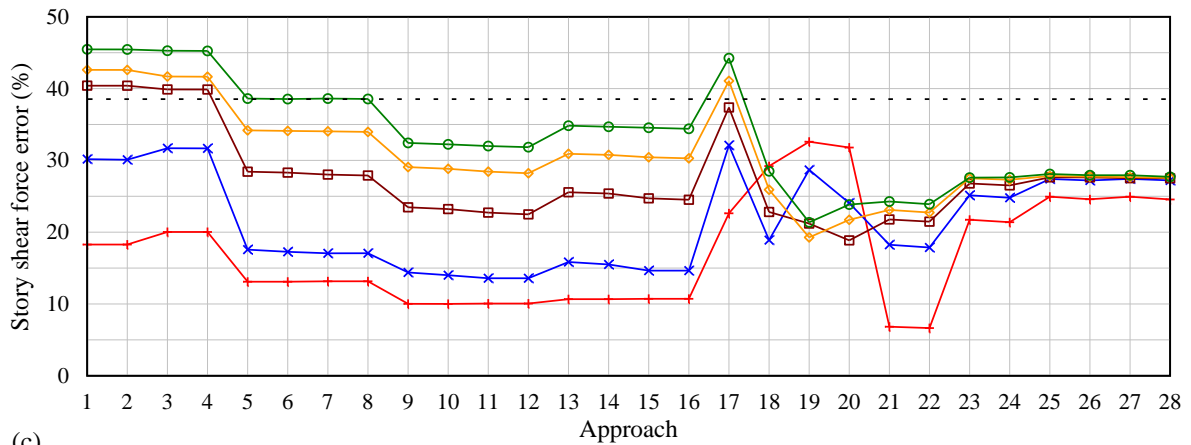
It is clearly seen from Fig. 3.3 that errors for a particular damping ratio using various approaches within any group other than Group E, do not show significant differences for all the response indicators. This implies that the choice of (a) higher mode (mode 3 or mode 4) frequency and (b) stiffness matrix (initial or tangent), in the application of viscous damping has negligible influence on the response indicators. The choice of stiffness matrix does not have a significant influence because stiffness-proportional damping constitutes a very small fraction of viscous damping, compared with mass-proportional damping. In addition, the fact that the stiffness of the superstructure is not changed significantly during the excitations also implies that the choice of stiffness matrix in the application of damping has negligible influence. This is different from fixed-base or base-isolated structures subjected to strong ground motions which result in significant stiffness degradation. The errors for a particular damping ratio using the approaches within Group E are significantly different. In addition, the error trends with respect to damping ratio are changed for Approaches 18–20 compared with other approaches. Although the related results are not shown here for brevity, it was found from the numerical analysis results that Approaches 18–20 underestimate the floor displacement response but overestimate the floor acceleration and story shear force responses for almost all the damping ratios. The floor displacement response using Approaches 18–20 were found to be slightly smaller than the corresponding Rayleigh damping counterparts, while the floor accelerations and story shear forces were significantly larger for all the damping ratios. This is because mass-proportional damping, which can be visualized as dampers connecting each mass to an external support, does not correspond to a realistic physical phenomenon (Pg. 455 Chopra 2007). Therefore, the application of only mass-proportional damping is not desirable. Here it is noted that although the mass-proportional damping dominates, the errors obtained using only the mass-proportional damping part of Approaches 1–16, are not the same errors when only mass-proportional damping is considered in Approaches 17–20, as the



(a)

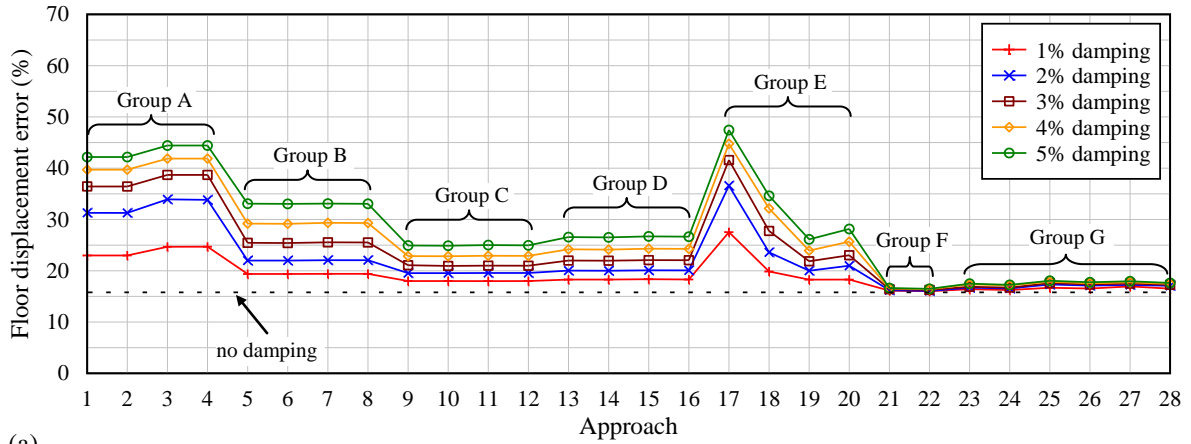


(b)

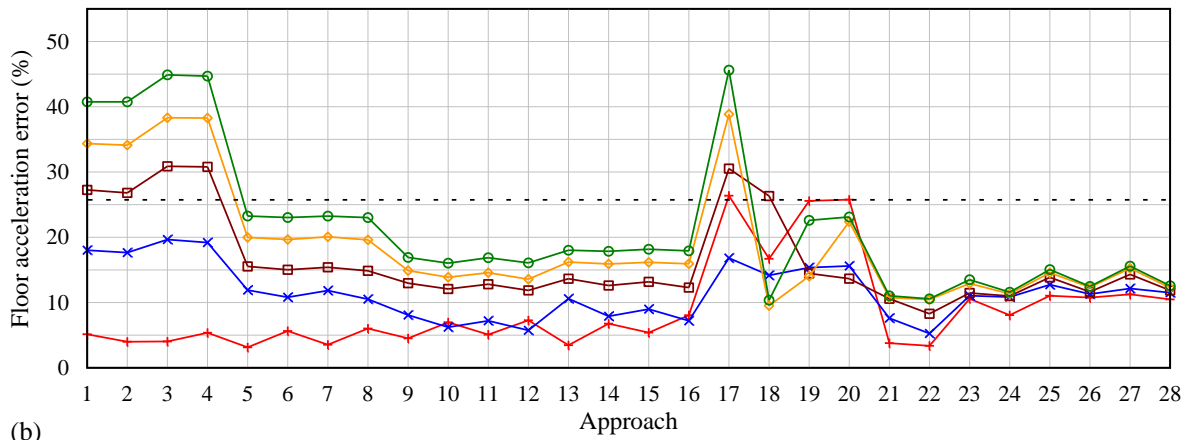


(c)

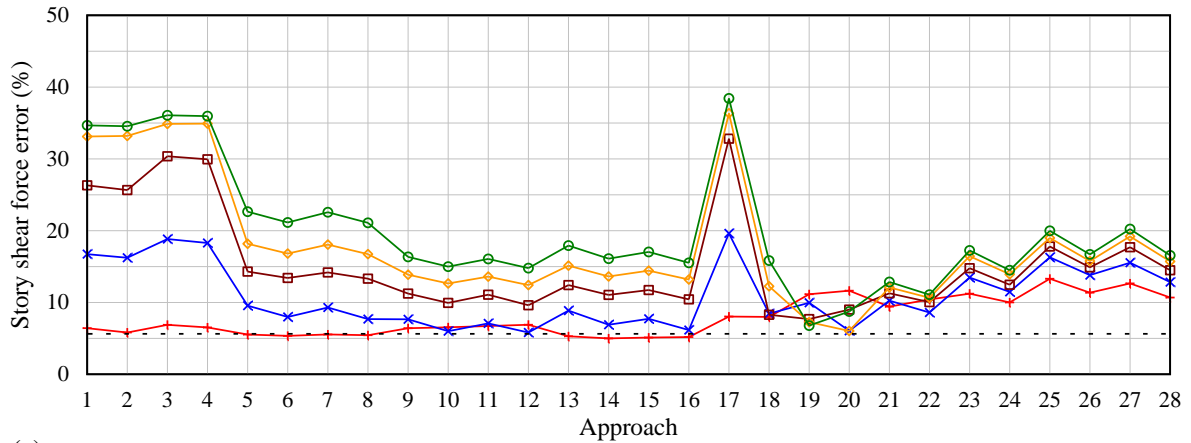
Fig. 3.2. Maximum errors in peak values of response indicators for all the stories for the ELC-S1 excitation: (a) relative floor displacement; (b) absolute floor acceleration; and (c) story shear force. The dashed line indicates the maximum error when viscous damping was not considered.



(a)



(b)



(c)

Fig. 3.3. Maximum errors in peak values of response indicators for all the stories for the MIYA-50 excitation: (a) relative floor displacement; (b) absolute floor acceleration; and (c) story shear force. The dashed line indicates the maximum error when viscous damping was not considered.

damping coefficient a_0 is computed using different equations. For example, for $\omega_1 = 37.14$ rad/s and $\omega_3 = 66.62$ rad/s ($\omega_4 = 130.62$ rad/s), $a_0 = 47.7\xi$ ($a_0 = 57.8\xi$) for the mass-proportional part of Rayleigh damping and $a_0 = 74.3\xi$ for only mass-proportional damping. Therefore, the damping coefficient for only mass-proportional damping is larger than that for the mass-proportional part of Rayleigh damping, which essentially results in higher degree of damping. Similar results were observed by Erduran (2012) for fixed-base steel buildings.

Another important observation from the results is that for the floor displacements, smallest errors occur when viscous damping was neglected in the model (Figs. 3.2(a) and 3.3(a)). However, Figs. 3.2(b), 3.2(c), and 3.3(b) suggest that neglecting such damping may lead to higher errors in terms of the floor accelerations and story shear forces. In certain scenarios, viscous damping is also desirable by analysis programs for purposes of numerical stability. In addition, the higher error due to a particular approach of modeling damping, results mainly because of the inclusion of higher degree of damping.

It is observed that the errors using the updated damping coefficients a_0 and a_1 are smaller compared with using constant a_0 and a_1 , and the differences are more obvious for higher damping ratios. For example, consider the errors using approaches in Group B (constant a_0 and a_1) and Group D (updated a_0 and a_1), where in the latter group the errors are smaller (Figs. 3.2 and 3.3). It is interesting to consider the results obtained using the approaches in Group C, where damping coefficients were computed based on the modal analysis of the base-isolated building with post-elastic stiffness of the isolation system. The errors using the approaches in Group C are either smaller than or comparable with the errors in Group D for all the damping ratios (Figs. 3.2 and 3.3). In addition, the analysis time with the approaches in Group C was found to be about one fourth of the analysis time using approaches in Group D, where damping coefficients were updated in each analysis step. Therefore, approaches in Group C are more attractive from the view point of computational cost than approaches in Group D.

The analysis results indicate that there is no unique *best approach* for the modeling of viscous damping suitable for all situations. The following two methods seem to yield the least errors:

Method 1: Group C type damping, i.e., Rayleigh damping, with the damping coefficients a_0 and a_1 computed from the frequencies of the base-isolated building with the post-elastic stiffness of the isolation system. However, it should be noted that with this type of damping, the errors depend greatly on the selected damping ratio ξ .

Method 2: Group F type damping, i.e., stiffness-proportional damping with damping coefficient a_1 computed from the frequency of the superstructure for a fixed-base condition. It should be noted that with this type of damping, the errors do not vary significantly depending on the selected damping ratio ξ , compared with the Group C type damping, indicating less uncertainty in the predicated response with the choice of ξ . Group F type damping also includes the approaches recommended by Ryan and Polanco (2008).

4. CONCLUDING REMARKS

The consequences of modeling viscous damping in base-isolated RC buildings are investigated, by using a three-story building tested on a shaking table. The study has led to the following conclusions and recommendations:

- (1) Damping ratio as well as the approach adopted to model damping is crucial because the floor displacements, floor accelerations, and story shear forces are affected significantly by it.

- (2) Application of Rayleigh damping where the damping coefficients a_0 and a_1 are calculated from the frequencies of the superstructure for a fixed-base condition (Group A) and mass-proportional damping (Group E) should be avoided, as these approaches could produce large errors in response predictions.
- (3) Rayleigh damping where damping coefficients a_0 and a_1 are calculated from the frequencies of the base-isolated building with the post-elastic stiffness of the isolation system instead of the initial stiffness of the isolation system (Group C), could be used. However, the damping ratio should be carefully selected, as the building response depends greatly on it. As an alternative, stiffness-proportional damping where the damping coefficient a_1 is computed from the frequency of the superstructure for a fixed-base condition (Group F) could be used; with this approach the building response does not depend significantly on the selected damping ratio.

ACKNOWLEDGEMENTS

The first author is pleased to acknowledge a Monbukagakusho (Ministry of Education, Culture, Sports, Science and Technology, Japan) scholarship for graduate students. Financial support from Center for Urban Earthquake Engineering (CUEE), Tokyo Institute of Technology is gratefully acknowledged.

REFERENCES

- Charney, F.A. (2008). Unintended consequences of modeling damping in structures. *Journal of Structural Engineering* (ASCE) **134:4**, 581-592.
- Chopra, A.K. (2007). *Dynamics of Structures: Theory and Applications to Earthquake Engineering*, Pearson Education: New Jersey.
- Clark, P.W., Aiken, I.D., and Kelly, J.M. (1997). Experimental studies of the ultimate behavior of seismically-isolated structures: Technical Report, UCB/EERC-97/18, Earthquake Engineering Research Center, University of California, Berkeley.
- Erduran, E. (2012). Evaluation of Rayleigh damping and its influence on engineering demand parameter estimates. *Earthquake Engineering and Structural Dynamics* (in press).
- Hall, J.F. (2006). Problems encountered from the use (or misuse) of Rayleigh damping. *Earthquake Engineering and Structural Dynamics* **35**, 525-545.
- Léger, P. and Dussault, S. (1992). Seismic-energy dissipation in MDOF structures. *Journal of Structural Engineering* (ASCE) **118:5**, 1251-1269.
- Menegotto, M. and Pinto, P. (1973). Methods of analysis for cyclically loaded R/C frames. *Symposium of Resistance and Ultimate Deformability of Structure Acted by Well Defined Repeated Load*, Lisbon, Portugal.
- OpenSees (2010). Open system for earthquake engineering simulation. Computer Program, University of California, Berkeley. Available from: <http://opensees.berkeley.edu>.
- Pant, D.R. and Wijeyewickrema, A.C. (2012). Structural performance of a base-isolated reinforced concrete building subjected to seismic pounding. *Earthquake Engineering and Structural Dynamics* (in press).
- Park, R., Priestley, M.J.N., and Gill, W.D. (1982). Ductility of square-confined concrete columns. *Journal of Structural Engineering* (ASCE) **108**, 929-950.
- Ryan, K.L. and Polanco, J. (2008). Problems with Rayleigh damping in base-isolated buildings. *Journal of Structural Engineering* (ASCE) **134:11**, 1780-1784.
- Yassin, M.H.M. (1994). Nonlinear analysis of prestressed concrete structures under monotonic and cyclic loads. *Ph.D. Dissertation*, University of California, Berkeley.